# Pterodactyl: Thermal Protection System Design Methodology for a Flap Control System

Zane B. Hays*,Veronica M. Hawke‡
*STC, Inc., Moffett Field, CA, 94035 Research Assistant, STC, Inc.*

Sarah N. D'Souza§, Bryan C. Yount **, David J. Kinney ***, and M. Kathleen McGuire ††
*NASA Ames Research Center, Moffett Field, CA, 94035*

**As interest in non-traditional entry vehicles continues to grow, the need for a Thermal Protection System (TPS) analysis approach that can account for entry solutions with changing geometry and complicated flow dynamics becomes invaluable. The NASA Space Technology Mission Directorate (STMD) Pterodactyl project aims to accomplish this through examination of a flap controlled Adaptable, Deployable Entry Placement Technology (ADEPT)-style Deployable Entry Vehicle (DEV). This paper details an improved methodology for modeling the aerothermodynamic environment and initial TPS design for a flap control system integrated with a symmetric DEV. Improvements include i) the addition of an anchoring process that uses an increased fidelity aerodynamic solution to anchor the aerothermal environment predictions and ii) increased surface resolution, for the 1D heat transfer analysis, to isolate the hottest area on the flap that will require the thickest TPS. It was found that the anchoring process provided an improved aerothermal environment prediction. Additionally, this analysis demonstrated that there is a need for increased surface resolution in the 1D thermal analysis since the predicted location of the hottest point was significantly different than the location identified using very coarse surface resolution.**

## I. Nomenclature

| | | |
|---|---|---|
| $\alpha$ | = | Angle of Attack (Alpha) |
| *ADEPT* | = | Adaptable, Deployable Entry Placement Technology |
| $\beta$ | = | Sideslip Angle (Beta) |
| *DEV* | = | Deployable Entry Vehicle |

* Junior Research Analyst, Systems Analysis Office, NASA ARC/AA, AIAA Member.
‡ Senior Research Scientist, Systems Analysis Office, NASA ARC/AA, AIAA Member.
§ Principal Investigator, Entry Systems and Vehicle Development Branch, NASA ARC/TSS, AIAA Associate Member.
** Experimental Facility Developer, Engineering Systems Division, NASA ARC/RE.
*** Flight System Engineer, Systems Analysis Office, NASA ARC/AA.
†† Aerospace Flight Systems, Systems Analysis Office, NASA ARC/AA.

*G&C* = Guidance and Controls
*HEEET* = Heatshield for Extreme Entry Environment Technology
*IL* = Insulative Layer
*TPS* = Thermal Protection System
*PBV* = Pterodactyl Baseline Vehicle
*RL* = Recessive layer
*UTTR* = Utah Test and Training Range

## II. Introduction

The Thermal Protection System (TPS) is a critical part of entry vehicle design and can significantly impact mission capabilities. During Pterodactyl's chosen mission, entry into Earth's atmosphere at lunar return speeds, the vehicle and its control flaps are exposed to extreme aerothermal and aerodynamic loading conditions. Traditional TPS analysis methods are effective for determining TPS thicknesses for a fixed geometry but are not suitable for a rapidly changing vehicle geometry such as Pterodactyl's articulating flap control system [1]. The challenging part of the current iteration of the Pterodactyl Baseline Vehicle II (PBV-II) is the eight rapidly actuating flaps moving in and out of the flow to control the vehicle throughout its trajectory. Thus, a method to determine the required TPS thickness was previously developed to deal with the changing flap orientation, high heating, and complex shock-shock interactions for the asymmetric Pterodactyl Baseline Vehicle I (PBV-I) discussed in [2]. However, it was determined that the fidelity of the shock-shock interactions and the thermal analysis needed to be improved. This paper discusses an improved TPS design methodology for the PBV-II flap control system.

## III. Vehicle and Trajectory Specifications

### A. Analysis Assumptions

The assumptions used were aimed at scoping the analysis to ensure a reasonable TPS thickness estimate while limiting the amount of computational time required. First, it was assumed that the flow interactions between flaps are decoupled, allowing analysis of individual flaps without having to account for adjacent flap interactions [3]. In addition, it was assumed that modeling five flap deflection angles across the full deflection range of -45 to 20 degrees provided sufficient resolution for linear interpolation of aerodynamic properties between discrete solutions. These two assumptions reduce the dynamic PVB-II geometry to five static geometry configurations, decreasing the required number of CFD simulations and associated computational cost [4]. Finally, due to the complexities of anchoring the aft environment to the aerodynamics solutions, in the wake, the aerothermal prediction and subsequent 1D thermal analysis was isolated to the windward side of the flap.

### B. Vehicle Geometry

The PBV-II aeroshell utilizes the Adaptable, Deployable Entry Placement Technology (ADEPT, [5]) and is designed to deliver a much larger payload than a traditional entry vehicle for a given launch vehicle size due to its deployable heat shield design shown in Figure 1.

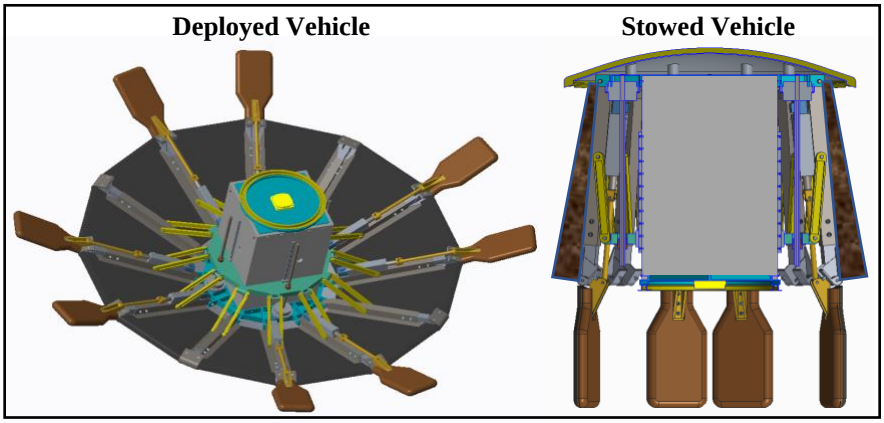


**Figure 1: PBV-II stowed and deployed**

Figure 2 demonstrates the flap designation around the vehicle, demonstrates flap deflection, and identifies the vehicle coordinate system. Note that the leading edge is defined as LE, the trailing edge is defined as TE, and the origin of the coordinate system is at the nose. To further clarify vehicle orientation, when the vehicle is lift vector up (angle of attack, $\alpha<0^o$), the trailing edge is pushed forward while the leading edge is pulled back.

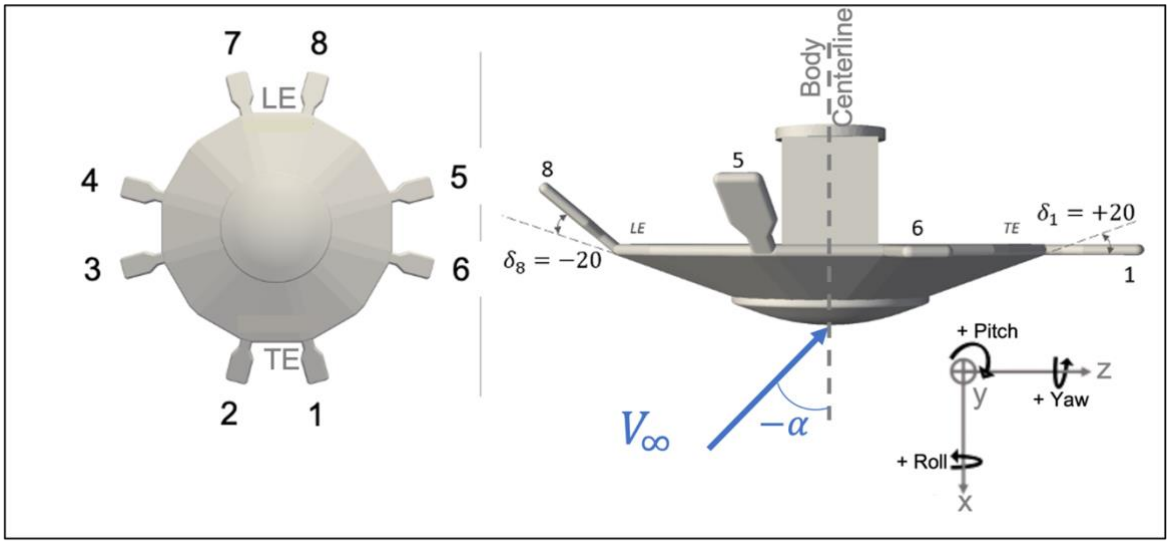


**Figure 2: Flap designation (left) and deflection definition with body coordinate system (right)**

Table 1 and Figure 3 briefly highlight the relevant geometric parameters for this vehicle configuration. Additional mechanical and geometric parameters can be found in D'Souza et al. [1].

**Table 1: Vehicle dimensions**

| Nose Radius (m) | Vehicle Diameter (m) | Cone Angle (deg.) | Estimated Total Mass (kg) |
|---|---|---|---|
| 1.43 | 2.86 | 70 | 703 |

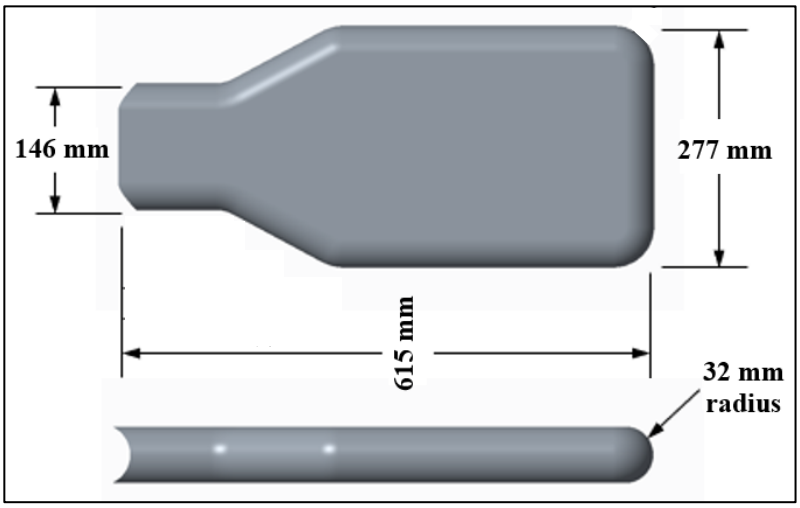


**Figure 3: Flap dimensions**

Using flaps to control the vehicle throughout the trajectory introduces an additional level of complexity to the TPS analysis process. Eight flaps that independently actuate in and out of the flow throughout the flight correspond to many complex geometry configurations that need to be analyzed. As discussed in the Assumptions section, five flap deflection geometries were selected for analysis and are pictured in Figure 4.

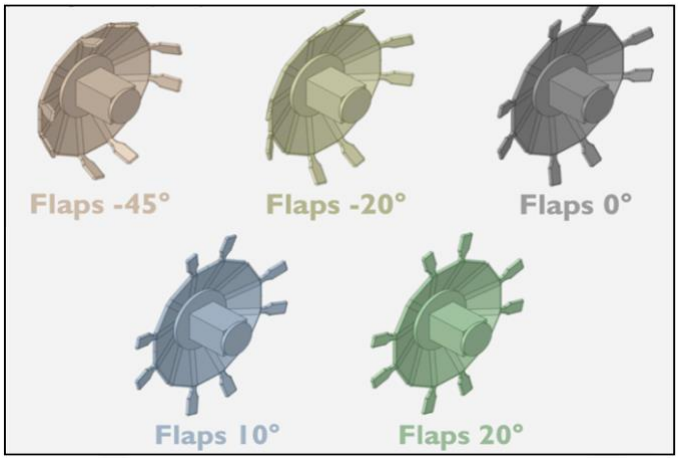


**Figure 4: Flap deflection angles**

After simulating the aerodynamic environment for each chosen geometry configuration, interpolation between the aerodynamic solutions was used to predict the flap aerothermal environments at unique deflection angles across the trajectory. The interpolation was performed using a Python library for Tensor-Product B-Splines (ndsplines) [6], which is particularly useful for multi-dimensional data sets such as aerodynamic data. This python library uses a piecewise linear B-Spline interpolation style was used.

### C. Aerodynamics, Controls, and Trajectory

The Pterodactyl lunar return concept of operations is detailed in [1] and is illustrated in Figure 5.

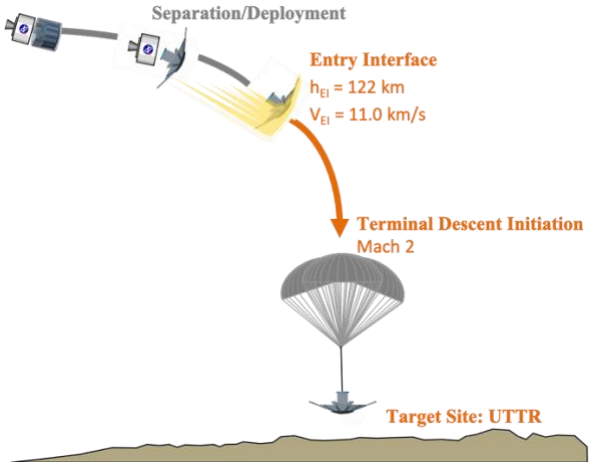


**Figure 5: Pterodactyl entry concept of operations**

A lunar return mission flies through a large variety of aerodynamic conditions and thus an aerodynamic solution space was developed to envelop these conditions. The aerodynamic bounds used for this solution space are discussed in [4] and summarized in Table 2 below.

**Table 2: Aerodynamic parameter bounds**

| Mach number | Dynamic Pressure {Pa} | Angle of Attack (α) {deg.} | Sideslip Angle (β) {deg.} |
|---|---|---|---|
| 2, 5, 10, 15, 20, 31, 40 | 1.16, 14.7, 129, 4710 | -10, -5, 0, 5, 10 | -10, -5, 0 |

The trajectory was developed as discussed in **Error! Reference source not found.**. Figure 6 shows the plots for Mach number (left, blue), dynamic pressure (left, orange), angle of attack (right, blue), and sideslip angle (right, orange). Note the double pressure spikes shown in Figure 6 (left, orange). These peaks are due to the vehicle completing a lofted trajectory, which is needed to burn off the energy from high entry speeds to meet the target range requirements. The angle of attack (α) and sideslip angle (β) profiles are found using an uncoupled range control

guidance algorithm that defines the guidance commands needed to meet range requirements and the terminal descent initiation at Mach 2. The negative β, throughout the trajectory, is needed to achieve the desired cross range objective. Angle of attack is negative (Lift vector up) for most of the trajectory and transitions to positive α (Lift vector down) towards the end to achieve down range requirements.

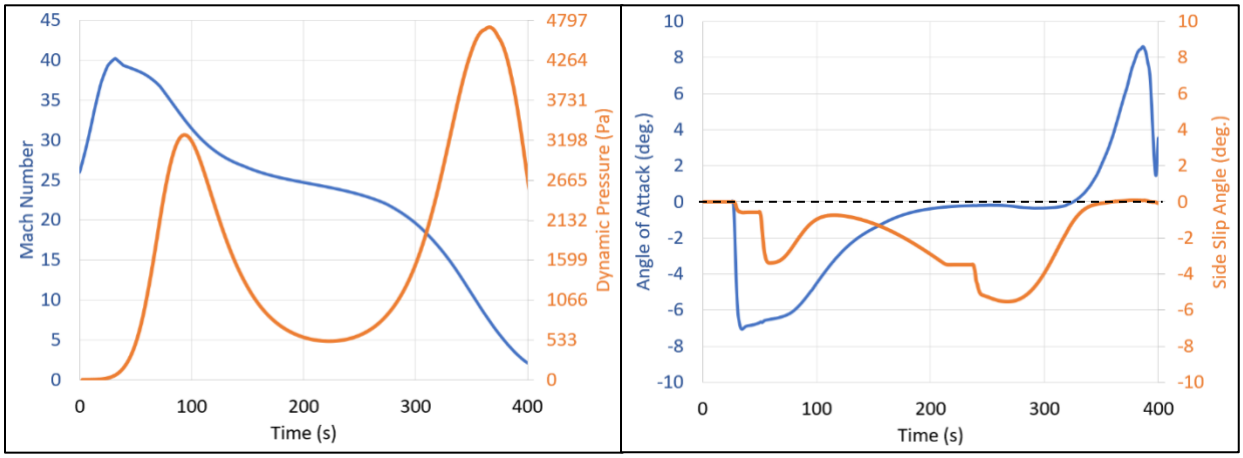


**Figure 6: Earth entry trajectory Mach Number and Dynamic Pressure (left) and vehicle guidance commands (right)**

Due to the negative β, one side of the vehicle is likely to experience higher heating than the other, in this case the side with flaps 2, 3, 4, and 7. A negative α exposes the leading edge of the vehicle such that flaps 1 and 2 are not directly exposed to the flow for much of the trajectory. However, it is expected that if any flap is deflected into the flow during high velocity and increasing dynamic pressure conditions, the heating environments around the flap will go up. The resulting flap deflection schedules are shown in Figure 7, **Error! Reference source not found.**.

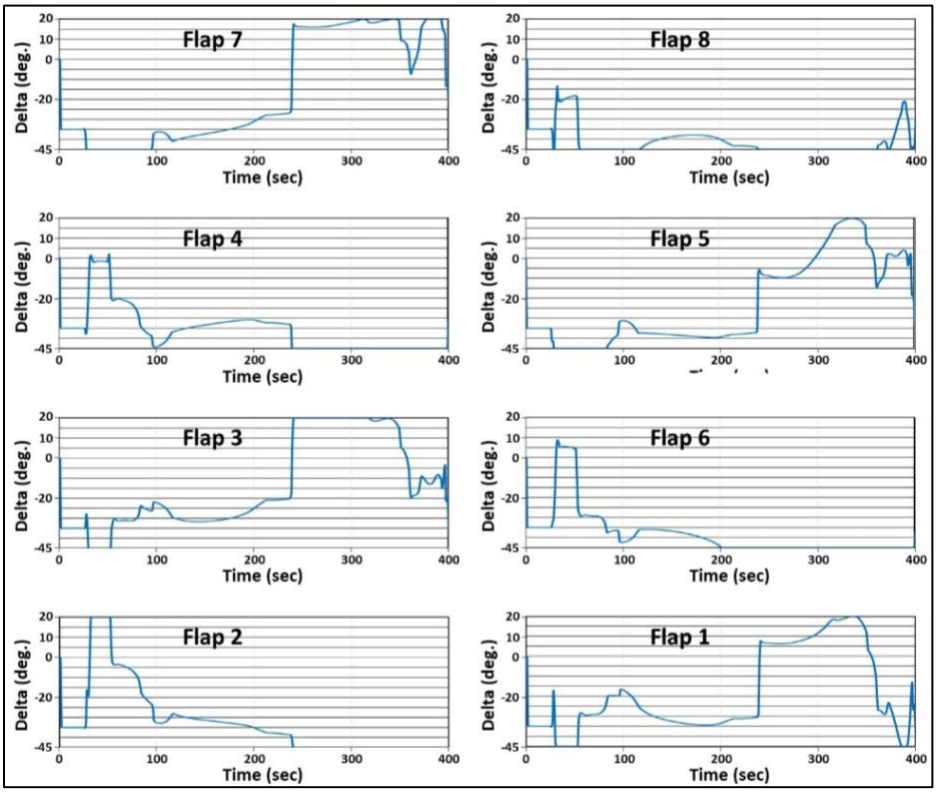


**Figure 7: Flap deflection angle schedule**

Notice the change in flap deflections at ~240 seconds, inducing the transition of $\alpha$ from negative to positive and $\beta$ transitioning to 0 degrees. Additionally, notice that in the first ~240 seconds, all the flaps are nominally deflected out of the flow (Delta<0°) with a few brief spikes to positive deflection angles. After ~240 seconds, flaps 1, 3, 5, and 7 are deflected at large positive angles (into the flow) for a prolonged amount of time, lofting the trajectory to burn entry energy and meet targeting requirements.

### D. Control Flap Material and Design

The high heating and velocities of the entry trajectory require a flap material capable of withstanding the heat rates and the pressures. Heatshield for Extreme Entry Environment Technology (HEEET) was chosen for this material and is discussed in [8]. HEEET is adequately suited to withstand high heating environments up to 3600 W/cm$^2$ [9] and can has suitable tensile properties to be used as a structural member. HEEET is a two-layer, 3D woven, carbon fabric infused with a phenolic resin to create a dense solid with an outer recession layer and an inner insulation layer. The HEEET material is molded around the titanium spar to form the flap shape, allowing the titanium spar to provide added rigidity to the flap structure Figure 8.

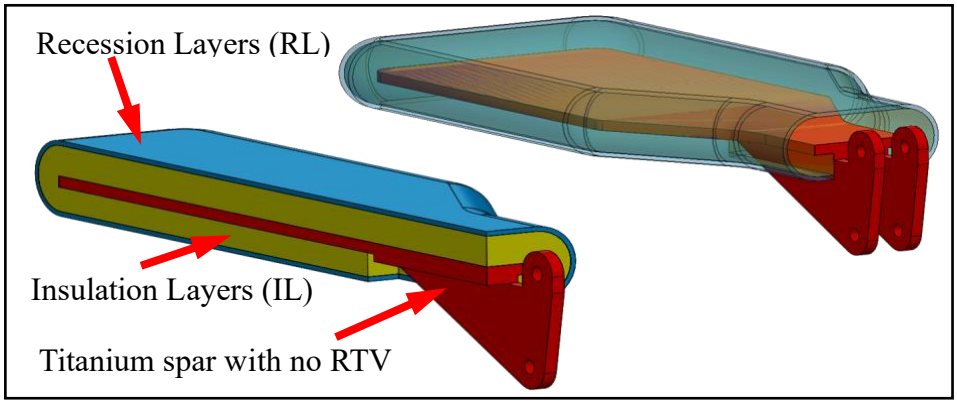


**Figure 8: HEEET flap design**

IL stands of insulation layer, RL stands for recession layer, and RTV stands for Room-Temperature vulcanized-rubber. RTV is an adhesive material commonly used in the space industry to bind materials together. The titanium spar provides a temperature and material boundary condition for the TPS analysis. A thermal limit of 589 kelvin was identified for the spar. The spar thickness is included in the analysis to determine the thermal mass, conductivity, and soak back. The spar is sized by the structural group as discussed in [1].

## IV. TPS Analysis Method Overview

The methodology used for this analysis was developed to extend the TPS analysis described in [2] and was broken into four phases (Figure 9). The primary differences in the new approach used for the PBV-II include, (a) the implementation of a high-fidelity method of anchoring CBAERO databases to high fidelity Cart3D inviscid aerodynamic solutions (Phases 1 and 2), (b) the addition of another iteration on the flap sizing with a fine grid across the surface of the flap (Phases 2 and 3), and (c) the addition of a 3D analysis discussed in [10] (Phase 4).

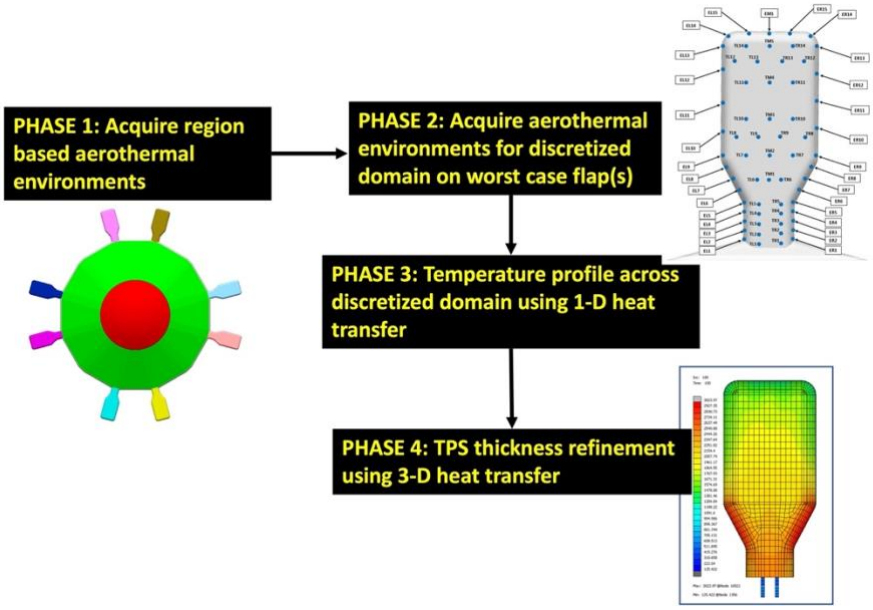


**Figure 9: Phased TPS analysis for Pterodactyl flap control system**

### A. Analysis Tools

As in the previous TPS analysis, the backbone of this process was built around two engineering-level analysis tools, CBAERO [11] and TPSSizer [12]. Additionally, an Equilibrium version of Cart3D [13] was utilized to generate higher fidelity aerodynamic solutions to adjust (anchor) the CBAERO database. The major change in the implementation of tools comes from a module of CBAERO (CBAERO-anchor) developed to facilitate the anchoring of a CBAERO database to a Cart3D database, discussed below in more detail.

### B. CBAERO Anchor

CBAERO-anchor was utilized to improve the fidelity of the CBAERO database with the increased realism of shock-shock interaction modeling in Cart3D aerodynamic solutions. The anchoring process involves creating two multidimensional database surfaces, one from the CBAERO data and the second from the Cart3D data. These surfaces are constructed from the Mach number, dynamic pressure, angle of attack, and sideslip angle parameters for each of the aerodynamic output parameters. Then a series of correction factors are created by taking either ratios or differences of two corresponding points on the pair of surfaces at a given aerodynamic condition. This process is discussed in more detail [14]. It is important to note that Cart3D does not predict heating and thus CBAERO does not directly anchor any of the heating parameters. Instead, the base aerodynamic parameters are anchored and then CBAERO calculates heating parameters from the anchored data. This analysis process increases the fidelity of the CBAERO heating data and ultimately that of the resulting TPS thickness predictions.

### C. Coarse Grid and Fine Grid Discretization

This section addresses the definition of a set of points on PBV-II for the thermal analysis tools, CBTPS and TPSsizer, and should not be confused with the meshes used for CART3D [4] or CBAero, which are different. A coarse grid and a fine grid were created in CBTPS to get the aero heating environments for TPSSizer. The primary purpose of having two different grid discretization's for the flap heating environments is to cut down on analysis time, since a fine grid across every flap would be computationally expensive. Therefore, it was decided to use a fine grid on the hottest flap(s) found in the coarse grid analysis, reducing computation time and capturing critical heating points. For the coarse grid, the windward face of each flap was discretized into a 5-point coarse grid to determine the flap with the greatest heating rate, complete a preliminary TPS sizing prediction and optimize the HEEET recession layer (Figure 9, Phase 1). Once the flap(s) with the most extreme heating environment were identified, a fine surface grid of 64 points was applied to the specific flap(s) to identify the peak heating location and provide understanding of the heating distribution across the windward surface of the flap (Figure 9, Phase 2). Flap surface discretizations and the resulting prediction for surface pressure distribution is shown in in Figure 10.

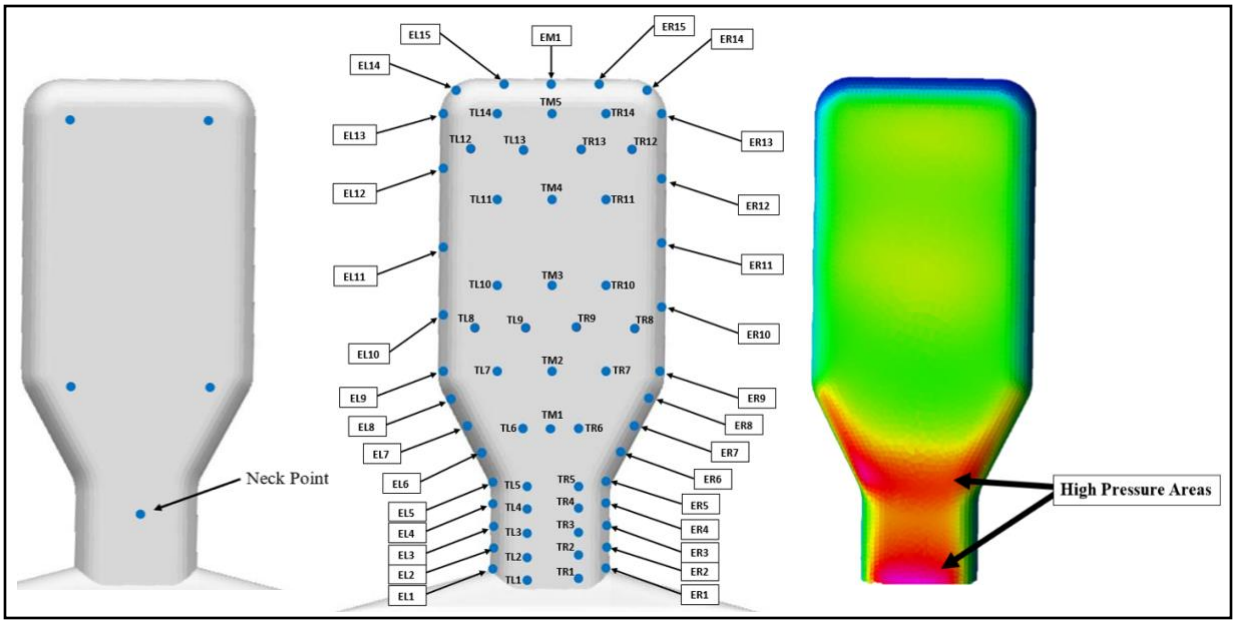


**Figure 10: Coarse grid (left), fine grid (middle), and example high pressure regions (right)**

The identified peak heating location on the coarse grid point is labeled as the Neck Point and was used for the preliminary sizing point as shown in Figure 10 (left). For the fine grid Figure 10 (middle), notice that there are more points clustered around the edges and the neck region of the flap. It was observed in the previous PBV-I analysis that higher magnitudes of pressure and heating occurred in these areas. In particular, when the flaps are deflected into the flow, a high-pressure region is seen on the edges of the neck region, Figure 10 (right). Note again that the grids illustrated in Figure 10 (left, middle) are only used to pull aeroheating data for use in sizing the TPS, these are not the grids used for CART3D or CBAERO.

## V. Flap TPS Analysis and Results

### A. Flap Database Anchoring and Aerodynamic heating

As the flaps are actuated in and out of the flow, it was determined that there would likely be shock interaction effects with the flaps. As CBAERO does not predict shock-shock interactions, Cart3D was used to anchor the CBAERO database. It is important to remember that Cart3D does not calculate heating and thus, CBAERO-anchor is only anchoring the base aerodynamic parameters. Pressure profiles were examined at several points along the trajectory and compared to the unanchored CBAERO data to ensure the anchoring process functioned as expected. Two of these cases are listed in Table 3 and are the two examples examined in this section.

**Table 3: CBAERO anchoring cases**

| *Case #* | Time (s) | Mach Number | $\alpha$ (deg.) | $\beta$ (deg.) | $\delta$ (deg.) |
|---|---|---|---|---|---|
| *1* | 29 | 40 | -5 | 0 | -45 |
| *2* | 296 | 20 | 0 | -5 | 20 |

These two anchoring cases correspond to conditions that occur during the two pressure pulses shown in Figure 6. As heating is largely a function of the vehicle's geometry and dynamic pressure, the points in Table 3 provide an understanding of the effects of modified Newtonian solutions from the unanchored CBAERO anchored to high-fidelity inviscid Card3D aerodynamics. Figure 11 shows the surface pressure for both the anchored and unanchored CBAERO, Case 1 and Case 2.

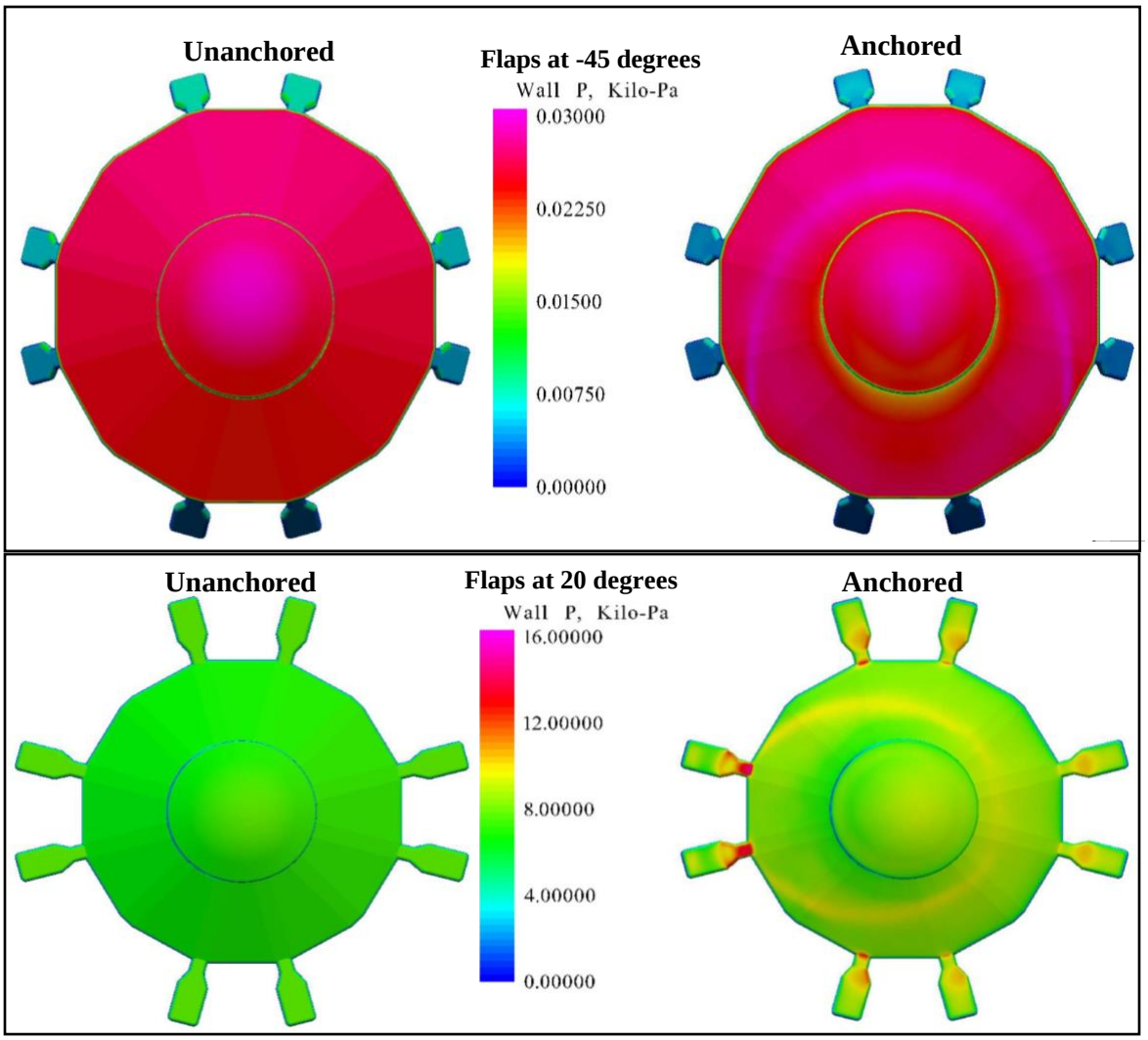


**Figure 11: Unanchored (left) and anchored (right) surface pressure distributions for Case 1 (top) Case 2 (bottom)**

Notice that the anchored cases show a high-pressure ring not seen by the unanchored cases because unanchored CBAERO does not capture complex flow phenomena. Notice the high-pressure regions seen on the flaps, due to shock-shock interactions captured by CART3D, in the Anchored (Cart3D-adjusted) plots as compared to the nearly constant pressure distribution seen in the Unanchored plots.

### B. Flap 1D TPS Prediction: Coarse and Fine Grid

First, examining the coarse grid heating environment data for all eight flaps, the convective heat rate is plotted in Figure 12. As the radiative heat rate is small in comparison to the convective heat rate, only the convective heat rate is considered. The convective heat rate informs the vehicle design as well as the G&C TPS limitations. It is also important to make sure that the heat rate remains below the threshold value for our chosen TPS material, HEEET.

Examining Figure 12, notice the effect of the flap deflection on the convective heat rate and recall controls and trajectory data discussed above. The larger the flap deflection during the dynamic pressure peaks, the larger the heat rates. Notice how flap 2 has a high deflection angle close to the peak dynamic pressure of the first pulse, resulting in a large convective heating spike. Interestingly, flap 6 has a similar rapid flap deflection into the flow but does not experience a resulting large convective heating spike because of the vehicle's $\alpha/\beta$ attitude. During the first heat pulse the vehicle is holding a consistent lift up and yaw to the right, thus flaps 2, 3, 4, and 7 have elevated heat rates as compared to the flaps 1, 6, 5, and 8 from being pushed more into the flow. Whereas the trend of the heat rate during the second dynamic pressure pulse is dictated by the control system commanding the flaps to reduce the sideslip and change the vehicle to a lift down orientation, causing flaps 1, 3, 5, and 7 to have larger heat rates than their counterparts.

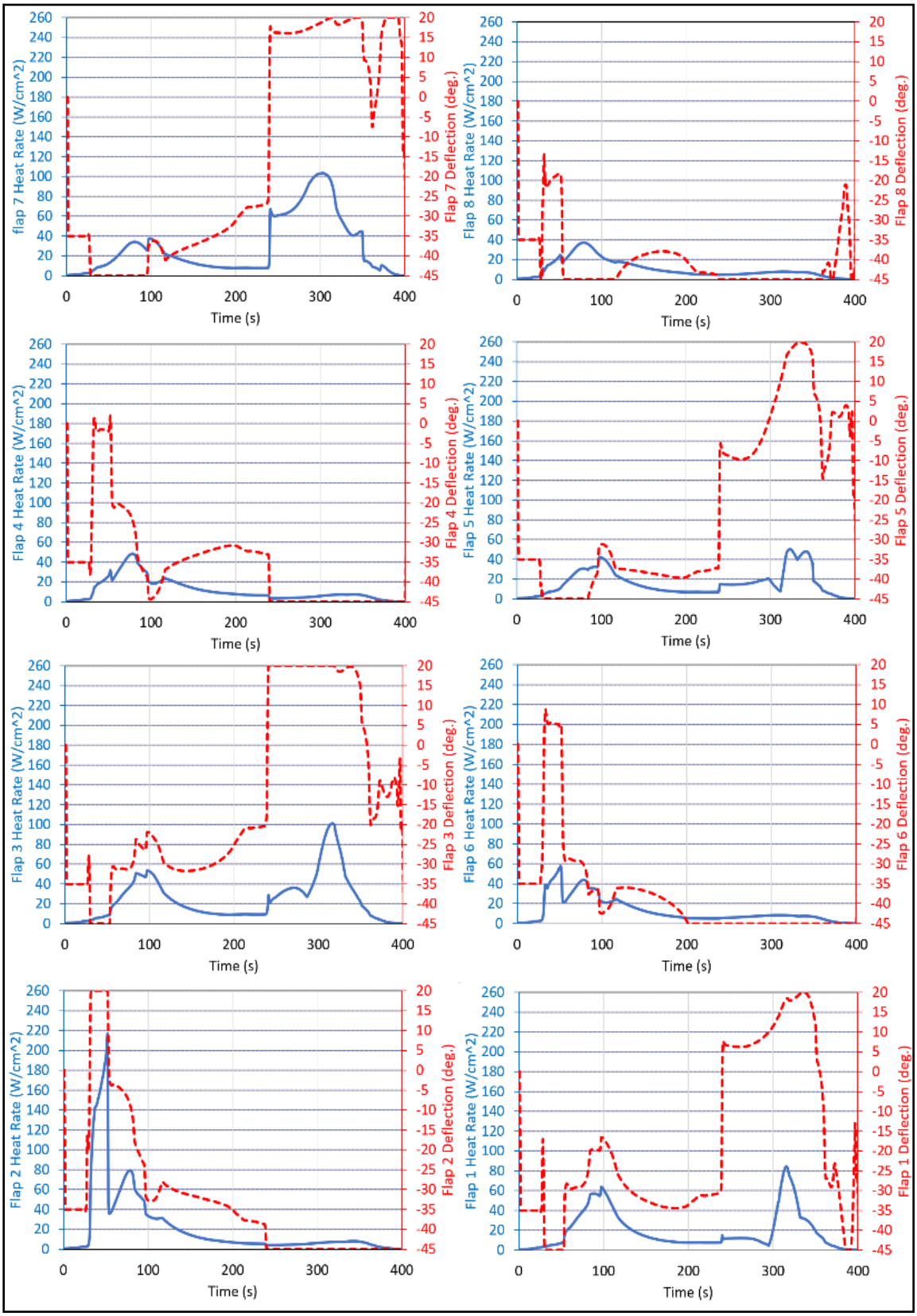


**Figure 12: Coarse grid convective heat rate and flap deflections**

Table 4 lists the maximum heat rate for each flap with respect to the corresponding aerodynamic conditions and vehicle orientations. The flaps with positive deflection angles, in general, result in large convective heat rates, as expected. The only noticeable exception to this observation is flap 5, but as discussed above the negative angle of attack and sideslip angle combined with the smaller Mach number are likely the primary causes of this lower maximum heating. Recall that the allowable heat rate for HEEET is 3000 W/cm$^2$ and the maximum convective heat rate spike of 216 W/cm$^2$, seen at flap 2, is well under the material limit. The relatively low heat rate on the flaps indicates that, if mechanical design dictated, a different TPS material could be considered. However, since a material with high tensile strength was required structurally and HEEET is a thermal protection system that also has good structural characteristics, it was decided to keep HEEET for this design.

**Table 4: Flap convective hear rates related to aerodynamic parameters**

| *Flap #* | Time (s) | $\dot{Q}_{conv}$ (W/cm$^2$) | Ma | q (Pa) | α (deg.) | β (deg.) | δ (deg.) |
|---|---|---|---|---|---|---|---|
| *1* | 314 | 84.47 | 17.7 | 2313 | -0.27 | -2.05 | 18.41 |
| ***2*** | **50** | **215.63** | **38.7** | **602** | **-6.66** | **-1.41** | **20.00** |
| *3* | 314 | 100.78 | 17.7 | 2313 | -0.27 | -2.05 | 20.00 |
| *4* | 76 | 48.60 | 35.9 | 2695 | -6.17 | -2.57 | -24.31 |
| *5* | 321 | 50.43 | 16.6 | 2738 | -0.11 | -1.27 | 17.73 |
| *6* | 49 | 57.97 | 38.8 | 551 | -6.70 | -0.78 | 4.80 |
| *7* | 301 | 103.25 | 19.5 | 1668 | -0.35 | -3.59 | 18.94 |
| *8* | 78 | 37.04 | 35.5 | 2833 | -6.08 | -2.39 | -45.00 |

The flap TPS design thicknesses based on coarse grid data can be seen in Figure 13 and are tabulated in Table 5 along with the integrated heat loads.

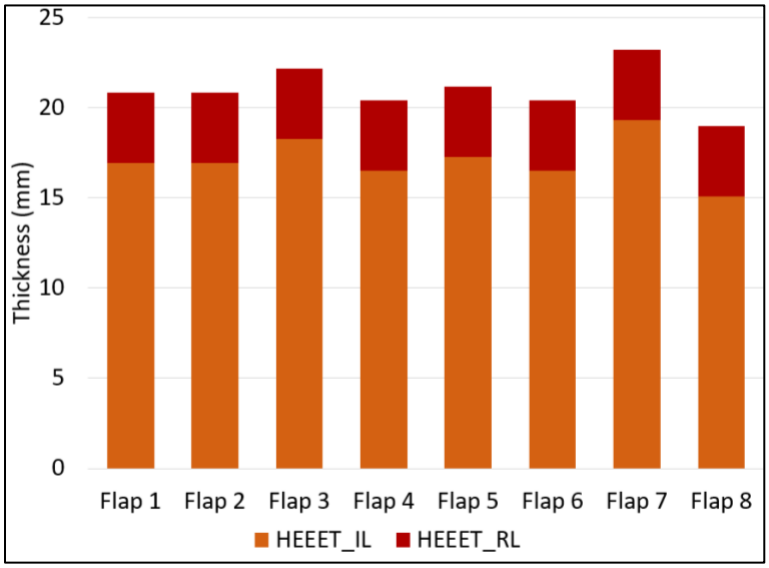


**Figure 13: Flap thickness from coarse grid analysis**

Note that even though flap 2 has a high convective heating spike, it is not the thickest flap since the thickness is driven by the integrated heat load not the magnitude of the convective heat rate. Flap 7 has the highest heat load, which is approximately ~1880 J/cm2 larger than the next highest heat load at flap 3. However, this resulted in only a 1 mm difference, between flap 7 and 3, in the estimated TPS thickness. This demonstrates a weak correlation between the heat load and required TPS thickness for the coarse grid approach used in TPSSizer. As a result, it was decided to run flaps 3 and 7 with a fine grid given the relative closeness of the TPS thickness estimates.

**Table 5: Flap thickness and integrated heat load**

| | Flap 1 | Flap 2 | Flap 3 | Flap 4 | Flap 5 | Flap 6 | Flap 7 | Flap 8 |
|---|---|---|---|---|---|---|---|---|
| *Total Thickness (mm)* | 20.9 | 20.9 | **22.2** | 20.4 | 21.2 | 20.4 | **23.2** | 19.0 |
| *Integrated Heat Load (J/cm$^2$)* | 7710 | 8734 | **9763** | 4627 | 6446 | 5156 | **11642** | 4128 |
| *Areal Mass (kg/m$^2$)* | 18.149 | 18.092 | **19.248** | 17.772 | 18.395 | 17.789 | **20.109** | 16.624 |

A fine grid was then defined on the windward surface of flaps 3 and 7, as discussed in the TPS Analysis Section above. The results from the fine grid are more accurate and the location of maximum integrated heat load was determined as shown by the red dot at the location named ER7 (Figure 14 (A)) for both flaps 3 and 7.

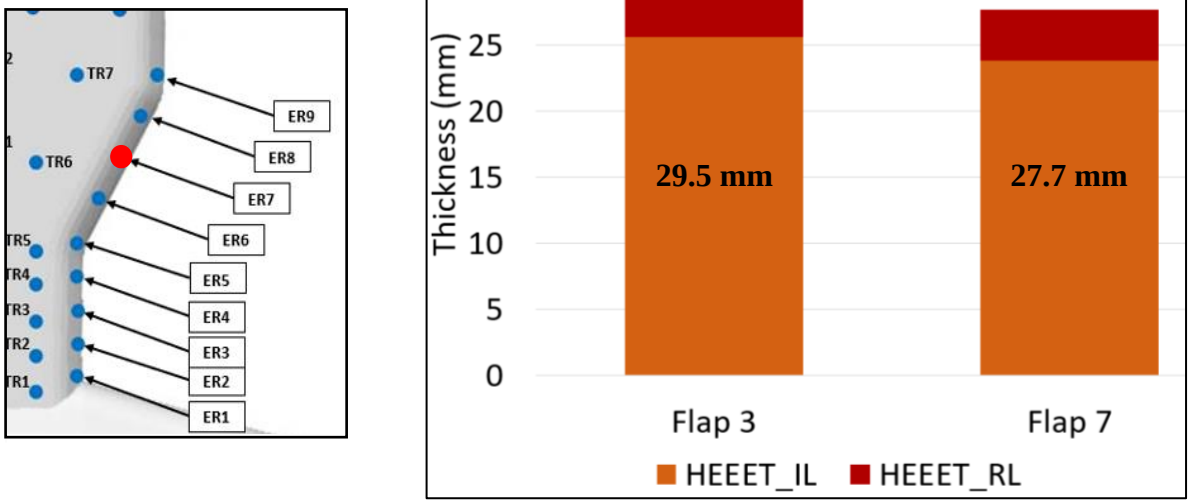


**(A)** **(B)**

**Figure 14: (A) Location of maximum integrated heat load for flaps 3 and 7, (B) Fine Grid Iteration TPS Thickness for Flap 3 and 7**

Figure 14 (B) plots the predicted TPS thickness for flaps 3 and 7 at the ER7 location. Notice that flap 3 is thicker than flap 7 which is opposite of what the coarse grid predicted . Additionally, the fine grid prediction is 6 mm thicker than the coarse grid prediction because it captured the highest heat load point on the side of the flap neck. The location of maximum heating changes significantly with different flap deflections, thus locating the critical point is difficult with a coarse grid alone. These results suggest that identifying a worst-case flap requires significant reduction in aeroheating environment uncertainty to ensure that the flap with the thickest TPS does not change with different grid fineness. Therefore, this process should be modified to apply a fine grid on all flaps.

## VI. Conclusions

The PBV-II analysis determined that a flap TPS thickness of 29.5 mm was required for adequate thermal protection. This TPS thickness estimate will be used, in Phase 4, for the 3D thermal analysis discussed in reference [10]. The maximum heat rate encountered by the flaps throughout the trajectory was ~215 W/cm$^2$, which is well below HEEET's functional limit of 3000 W/cm$^2$. Additionally, several observations on how control inputs and aerodynamic conditions affected heating on the control flaps were obtained. Namely, care should be taken when deflecting the flaps into the flow during high Mach number and high dynamic pressure regions of the trajectory to reduce mechanical design complexity and increase flap survivability. This paper successfully demonstrated a feasible methodology to define the aeroheating environments around a flap and perform initial thickness predictions for the flap TPS. The PBV-II TPS design methodology extended existing CBAERO TPSSizer capabilities to account for multiple flap deflection angles and sideslip angles. In addition, the inclusion of anchoring CBAERO to the inviscid Cart3D solutions began to reduce the uncertainties in the aerothermal environment predictions. But it was found that significant reductions in these uncertainties are still needed to ensure that the flap with the thickest TPS can be identified. Therefore, this process should be modified to apply a fine grid on all flaps. As interest in non-traditional entry vehicles continues to grow, the

application of this innovative TPS analysis will provide feasible solutions for a variable geometry exposed to entry flow dynamics.

## VII. Pterodactyl Future TPS Work

There are several areas of research that the Pterodactyl's TPS group would like to explore in the future. These items are aimed at increasing understanding of the problem, reducing uncertainties, and increasing the scope and detail of the TPS analysis. First, as discussed above, the fine grid TPS analysis solutions showed that while the first iteration got closer to a feasible solution, this tool can be further improved to better understand the differences between each of the flaps in the flow environment. The TPS group would like to pursue an anchoring that goes beyond Cart3D, this would include: i) performing an in-depth investigation of the accuracy of the anchored aerodynamics and ii) utilizing other higher fidelity analysis tools to capture boundary layer effects and allow anchoring of the heating parameters directly.

## Acknowledgments

The authors of this paper would like to thank NASA Space Technology Mission Directorate's Early Career Initiative (ECI) program for guiding and funding this work. Special thanks to the ECI Program Executive Ricky Howard and our ECI mentor Michelle Munk. We would also like to thank our collaborators at NASA Ames Research Center: Susie Go, Ken Gee, Michael Schuh, Antonella Alunni, Breanna Johnson, Wendy Okolo, Bryan Yount, Benjamin Margolis, Alan Cassell, Andrew Torricelli, Sander Visser, Don Ellerby, Milad Mahzari, Frank Milos, Owen Nishioka, and Keith Peterson.

## References

[1] D'Souza, S. N., Alunni, A. I., Yount, B. C., Okolo, W. A., Margolis, B. W., Hibbard, K.E., Barton, J. D., Hawke, V., Hays, Z. B., and Reddish, B. J., "Pterodactyl: System Analysis of an Asymmetric and Symmetric Deployable Entry Vehicle for Precision Targeting Using Flaps," *AIAA SciTech Forum*, Virtual: AIAA, 2021.

[2] Hays, Z. B., Yount, B. C., Nikaido, B. E., Tran, J., D'Souza, S. N., Kinney, D. J., and McGuire, M. K., "Pterodactyl: Thermal Protection System for Integrated Control Design of a Mechanically Deployed Entry Vehicle," *AIAA SciTech 2020 Forum*, AIAA, Orlando, FL, 2020.

[3] Nikaido, B. E., D'Souza, S. N., Hays, Z. B., and Reddish, B. J., "Pterodactyl: Aerodynamic and Aeroheating Database Development for Integrated Control Design of a Mechanically Deployed Entry Vehicle," *AIAA SciTech 2020 Forum*, AIAA, Orlando, FL, 2020.

[4] Reddish, B. J., Nikaido, B. E., D'Souza, S. N., Hawke, V., and Kang, H., "Pterodactyl: Aerodynamic Modeling for a Symmetric Deployable Earth Entry Vehicle with Flaps," AIAA SciTech 2021 Forum, AIAA, 2021.

[5] Venkatapathy, E., Hamm, K. R., Fernandez, I., Arnold, J., Kinney, D., Laub, B., Makino, A., McGuire, M. K., Peterson, K., Prabhu. D., Empey D., Dupzyk I., Huynh L., Hajela P., Gage P., Howard A., Andrews D., "Adaptive Deployable Entry and Placement Technology (ADEPT): A Feasibility Study for Human Missions to Mars," *21st AIAA Aerodynamic Decelerator Systems Technology Conference and Seminar*, AIAA 2011-2608, Dublin, Ireland, 2011.

[6] Margolis, B. W. L., Lyons, K. R., "ndsplines: A Python Library for Tensor-Product B-Splines of Arbitrary Dimension," The *Journal of Open Source Software*, JOSS, 25 Oct. 2019.

[7] Okolo, W. A., Margolis, B. W., Johnson, B. J., D'Souza, S. N., "Pterodactyl: Guidance and Control of a Symmetric Deployable Entry Vehicle using an Aerodynamic Control System," AIAA SciTech 2021 Forum, AIAA, 2021.

[8] Milos, F. S., Chen, Y., Mahzari, M., "Arcjet Tests and Thermal Response Analysis for Dual-Layer Woven Carbon Phenolic," *Journal of Spacecraft and Rockets*, Vol. 55, No. 3, May-June 2018.

[9] Gage, P., Mahzari, M., Peterson, K., Ellerby, D., Venkatapathy, E., "Technology Readiness Assessment for HEEET TPS," 16th International Planetary Probe Workshop, Oxford, UK, 2019.

[10] D'Souza, S.N., McGuire, M. K., S. N., Torricelli, A., Visser, S., Hays, Z. B., "Pterodactyl: 3D Thermal Analysis of an Aerodynamic Control System for a Symmetric Deployable Entry Vehicle," *AIAA SciTech 2022 Forum*, AIAA, 2022 (to be published).

[11] CBAERO, Configuration Based Aerodynamics, Software Package, Ver. 5.3.3, NASA Ames Research Center, Moffett Field, CA 2019.

[12] TPSSizer, Software Package, Ver. 3.5a, NASA Ames Research Center, Moffett Field, CA 2019.

[13] Cart3D, Software Package, Ver. 1.5.5, NASA Ames Research Center, Moffett Field, CA, 2019.

[14] Kinney, D. J., "Aerothermal Anchoring of CBAERO Using High Fidelity CFD," *45th AIAA Aerospace Sciences Meeting and Exhibit*, 2007.